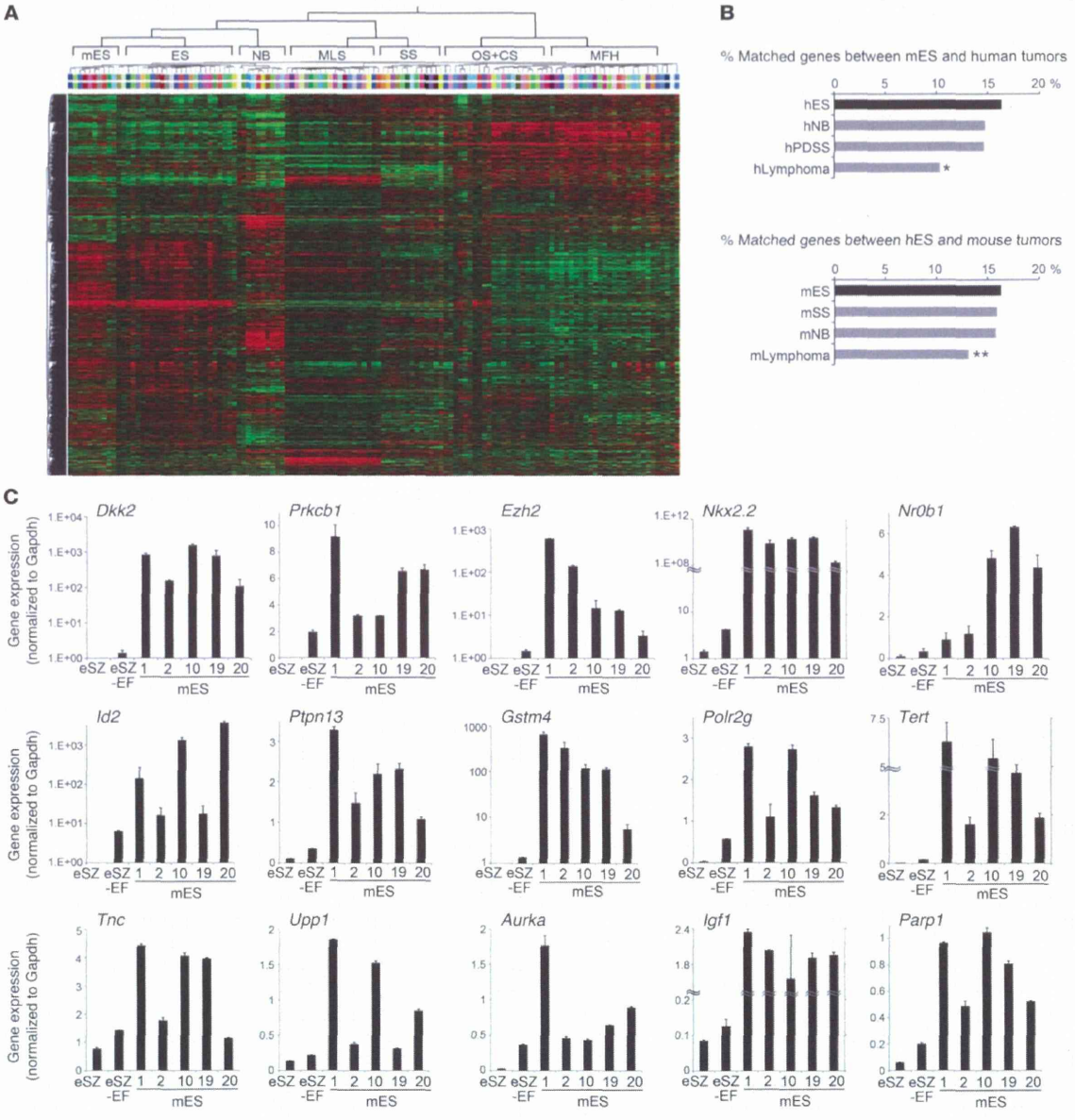

Figure 4

Clustering analysis of murine and human sarcomas. (**A**) Supervised clustering of gene expression profiles of 10 samples of murine Ewing's sarcomas (mES), 32 cases of human Ewing's sarcomas (ES), 21 malignant fibrous histiocytomas (MFH), 20 myxoid liposarcomas (MLS), 16 synovial sarcomas (SS), 11 osteosarcomas (OS), 10 neuroblastomas (NB) and 7 chondrosarcomas (CS). (**B**) Gene expression profiles of mouse and human Ewing's sarcoma (hES) were compared with those of other small round cell tumors of the other species. The frequencies of matched genes in 2,000 gene sets are indicated. Expression profiles of 6 human poorly differentiated synovial sarcoma (hPDSS) cases, 14 cases of human malignant lymphoma, 5 samples of murine synovial sarcoma, 7 murine neuroblastomas, and 6 murine malignant lymphoma were examined. (**C**) Quantitative RT-PCR for upregulated genes common between eSZ cells with *EWS-FLI1* (EF) and murine Ewing's sarcomas. The numbers listed above "mES" denote tumor IDs. The mean ± SEM of 3 independent experiments are shown. $^{*}P < 0.001$ vs. hES; $^{**}P < 0.01$ vs. mES.

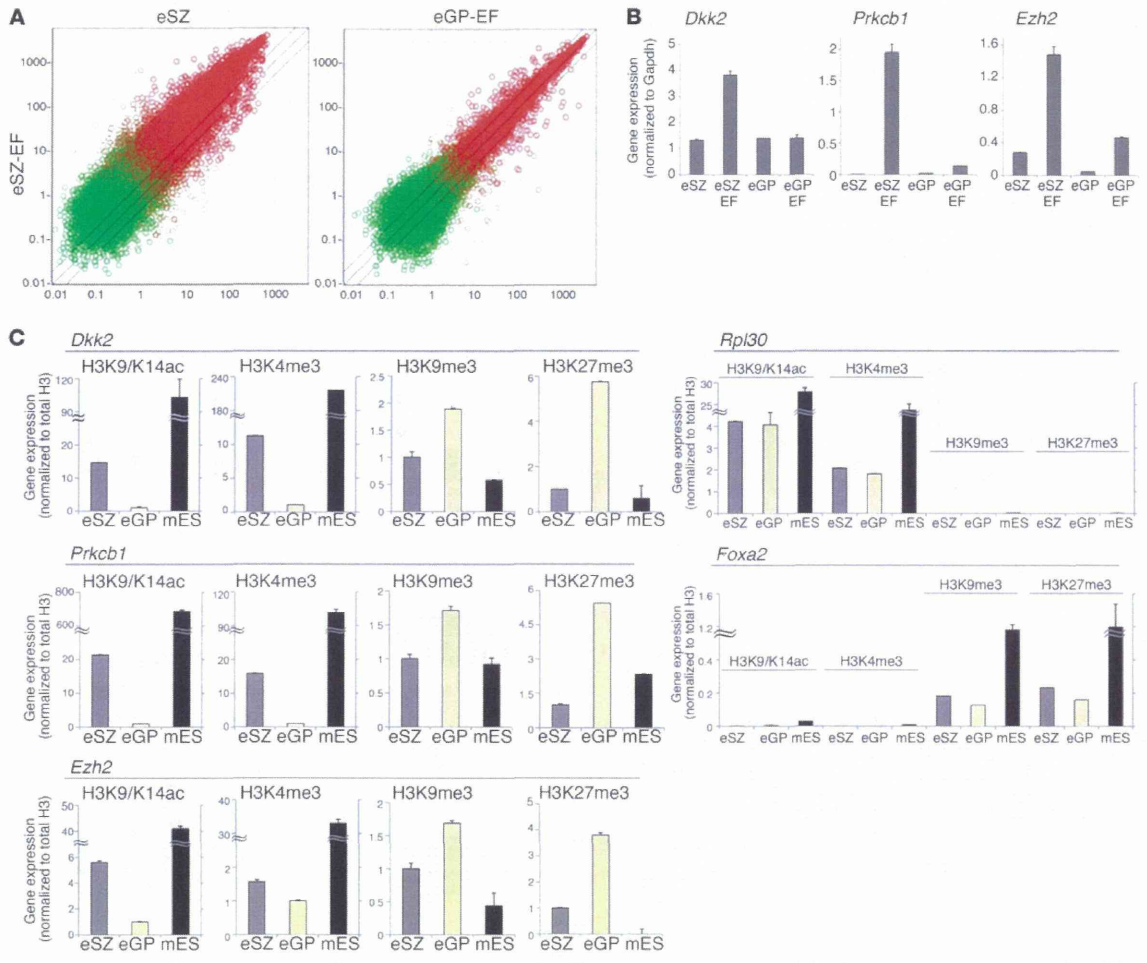

Figure 5

Differences in gene expression between eSZ and eGP cells. (**A**) Comparison of gene expression profiles between eSZ/*EWS-FLI1* and eSZ and eSZ/*EWS-FLI1* and eGP/*EWS-FLI1* 48 hours after introduction. Scatter plots of eSZ with (vertical axis) or without *EWS-FLI1* (horizontal axis) and eSZ with *EWS-FLI1* (vertical axis) or eGP with *EWS-FLI1* (horizontal axis) are shown. Red dots indicate probes of present call, and green dots indicate those of absent call. The threshold lines above and below the diagonal indicate $y = 2x$ (2-fold increase) and $y = 0.5x$ (2-fold decrease), respectively. (**B**) Expression patterns of *Dkk2*, *Prkcb1*, and *Ezh2* were validated by quantitative RT-PCR. The mean ± SEM of 3 independent experiments are shown. (**C**) ChIP-PCR for histone modification at *Dkk2*, *Prkcb1*, and *Ezh2* promoter regions in eSZ, eGP, and murine Ewing's sarcomas. *Rpl30* and *Foxa2* were used as controls for active and repressive histone marks, respectively. The mean ± SEM of 3 independent experiments are shown.

hood. This scenario explains why the location of Ewing's sarcoma is different from that of osteosarcoma, which is frequently observed in the metaphysis of long bones. There is a variant of human Ewing's sarcoma that develops in the soft tissue and is also characterized by the invariable *EWS-ETS* fusion. As the origin of Ewing's sarcoma in the soft tissue remains to be clarified, the relatively late onset of the tumor suggests that dysregulation of the differentiation program in the mesenchymal system might play some role in its tumorigenesis.

Upregulation of the WNT/β-catenin pathway is a direct effect of EWS-ETS expression in preneoplastic and sarcoma cells, at least in part. However, rather mild β-catenin induction by EWS-FLI1 in the eSZ (Supplemental Figure 9A) suggests that additional genetic events might be required for constitutive activation of the pathway. Pathways involving receptor tyrosine kinases are also important in Ewing's sarcoma (40, 51), as was indicated in our model. Indeed, potential clinical benefits from the use of pazopanib, a multikinase inhibitor, for the treatment of childhood sarcoma, including Ewing's sarcoma, have been reported recently (52).

Tumor formation in our mouse model of Ewing's sarcoma was *EWS-ETS* dependent, as was clearly exhibited by *Cre/loxP*-mediated knockout experiments. This finding suggests that therapeutic

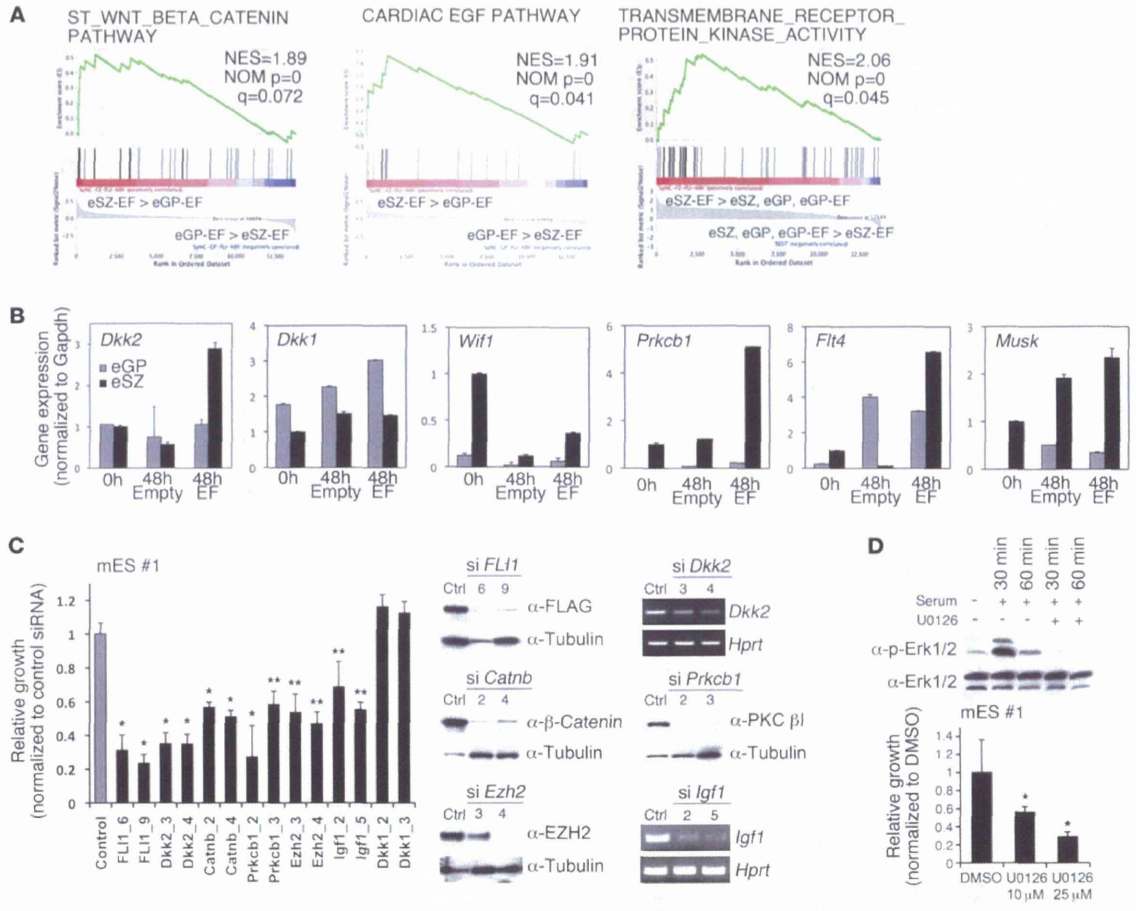

Figure 6

Modulation of gene expression and growth suppression of tumor cells by gene silencing. (**A**) GSEA of eSZ and eGP cells with *EWS-FLI1* (left and central panels) and between eSZ/*EWS-FLI1* and eGP, eSZ, and eGP/*EWS-FLI1* (right) resulted in enrichment of the WNT/β-catenin pathway, the EGF pathway, and receptor tyrosine kinase activities. (**B**) Real-time quantitative RT-PCR for *Dkk2*, *Dkk1*, *Wif1*, *Prkcb1*, *Flt4*, and *Musk* in eSZ or eGP cells with/without *EWS-FLI1* at 0 or 48 hours after introduction. The mean ± SEM of 3 independent experiments are shown. (**C**) Inhibition of cell proliferation by knockdown of *EWS-FLI1* and genes of the pathways specified in **A**. Relative growth of tumor cells 48 hours after siRNA treatment was calculated by comparing each cell number to cells treated with control siRNA. The symbols of siRNA used are indicated. *Dkk1* was tested as a negative control. Gene knockdown was confirmed by immunoblotting (*Fli1*, *Catnb*, *Ezh2*, and *Prkcb1*) or RT-PCR (*Dkk2* and *Igf1*). The experiment was repeated 3 times, and representative results are shown. (**D**) Effect of MAPK pathway inhibition on tumor growth. Erk phosphorylation was inhibited by a MEK1/2 inhibitor U0126 (10 μM) (top), and tumor proliferation was inhibited in a dose-dependent manner 48 hours after treatment (bottom). The mean ± SEM of 3 independent experiments are shown. $^{*}P < 0.01$; $^{**}P < 0.02$.

approaches should pursue the direct targeting of EWS-ETS as well as related pathways. Gene knockdown experiments and screening of inhibitory drugs in our model should prove valuable. Unlike the xenograft model of human cancer cells, the present mouse model excludes the unexpected bias caused by rather low penetrance of transplantation, an altered relationship between tumor cells and the microenvironment, and defects in certain signaling pathways due to differences in species-dependent binding affinities between ligands and receptors. Thus, our platform will allow us to explore and evaluate novel targeted therapies in combination with tests using human Ewing's sarcoma cell lines.

In summary, purification of the targets of primary oncogenic stimuli permitted us to establish a mouse model that closely recapitulates important characteristics of human Ewing's sarcoma. Taken together, the efficiency of tumor induction and the gene expression analyses of both the very limited cell population obtained by laser microdissection and the early neoplastic lesion strongly suggest that the cell of origin of Ewing's sarcoma is enriched in the eSZ cells. The present ex vivo method could be useful for generating other important animal models for human cancers, particularly when conventional transgenic models are driven by a gene expression-based method that is not always successful at

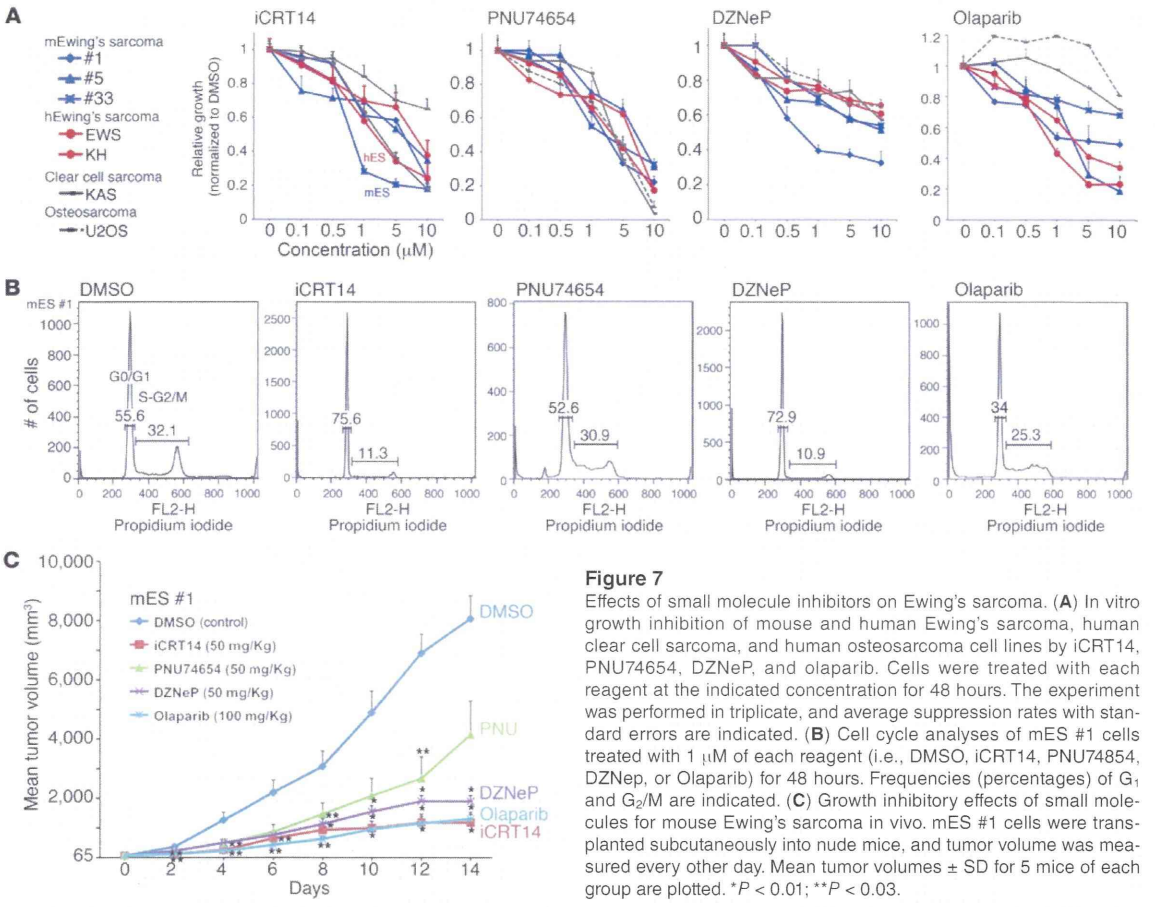

Figure 7

Effects of small molecule inhibitors on Ewing's sarcoma. (**A**) In vitro growth inhibition of mouse and human Ewing's sarcoma, human clear cell sarcoma, and human osteosarcoma cell lines by iCRT14, PNU74654, DZNeP, and olaparib. Cells were treated with each reagent at the indicated concentration for 48 hours. The experiment was performed in triplicate, and average suppression rates with standard errors are indicated. (**B**) Cell cycle analyses of mES #1 cells treated with 1 μM of each reagent (i.e., DMSO, iCRT14, PNU74854, DZNep, or Olaparib) for 48 hours. Frequencies (percentages) of G_1 and G_2/M are indicated. (**C**) Growth inhibitory effects of small molecules for mouse Ewing's sarcoma in vivo. mES #1 cells were transplanted subcutaneously into nude mice, and tumor volume was measured every other day. Mean tumor volumes ± SD for 5 mice of each group are plotted. $^*P < 0.01$; $^{**}P < 0.03$.

targeting exact cell types. The plasticity of precursor cells as well as their oncogenic potency due to chimeric transcription factors can be evaluated by the present approach and constitutes a useful tool for clarifying oncogenic mechanisms of childhood cancer.

Methods

Purification of eSZ cells. Femoral and humeral bones of BALB/c mouse embryos were removed aseptically on 18.5 dpc, and they were microdissected into eSZ, eGP, and eSyR under a stereomicroscope (Zeiss Stemi 2000-C, Carl Zeiss MicroImaging). Embryonic mesenchymal cells of the head or trunk were also prepared from the same embryos during each experiment. Each region was minced and gently digested with 2 mg/ml collagenase (Wako Pure Chemical) at 37°C for 2 hours. They were cultured in growth medium composed of Iscove's Modified Dulbecco's Medium (Invitrogen) supplemented with 15% fetal bovine serum and subjected immediately to retroviral infection. Fractionation of PTHLH$^-$ and PTHLH$^+$ eSZ populations was achieved using a rabbit anti-PTHLH (Abcam) and a CELLection Biotin Binder Kit (Dynal) according to the manufacturer's protocol. The frequency of the PTHLH$^-$ cells reached 8.3% of total eSZ cells (12-fold enrichment).

Retroviral infection and transplantation. N-terminal FLAG-tagged *EWS-FLI1* and *EWS-ERG* were introduced into the pMYs-IRES-GFP or pMYs-IRES-Neo vectors. The full-length *EWS-FLI1* cDNA was a gift from Susanne Baker (St. Jude Children's Research Hospital, Memphis, Tennessee, USA), and *EWS-ERG* was cloned from a human Ewing's sarcoma case. Retroviral infections of eSZ, eGP, or shaft cells were performed as described previously (53). Infection efficiency was examined using a FACSCalibur flow cytometer (Becton Dickinson). After 48 hours of spin infection, the cells were mixed with growth factor–reduced Matrigel (Becton Dickinson) and were transplanted subcutaneously to BALB/c nude mice. The mice were observed daily to check for tumor formation and general condition. Tumors were resected and subjected to further examination when subcutaneous masses reached 15 mm in diameter. Some tumors (1×10^6 cells) were serially transplanted subcutaneously or injected into the tail veins (1×10^6 cells) of nude mice to confirm tumorigenicity and metastatic activities.

Histopathology and immunohistochemistry. Formaldehyde- or paraformaldehyde-fixed tumor tissues were embedded in paraffin, and sections were stained with hematoxylin and eosin using standard techniques. Bromodeoxyuridine (BrdU) labeling was achieved by intraperitoneal injection of 1 mg/ml BrdU 30 minutes before sacrifice. eSZ cells were cultured on chamber slides and were fixed with 100% methanol. EWS-FLI1 and EWS-ERG antigens were detected using a polyclonal rabbit anti-FLAG antibody (Sigma-Aldrich) in conjunction with the VECTOR M.O.M. Immunodetection Kit (Vector Laboratories) or FITC-conjugated anti-rabbit immunoglobulin. The following primary antibodies were used: anti-BrdU (Molecular

Table 3
IC_{50} values of inhibitors

	Inhibitors			
Tumor cells	iCRT14 (μM)	PNU74654 (μM)	DZNeP (μM)	Olaparib (μM)
mES #1	5.90	2.08	0.68	7.07
mES #5	5.61	6.79	10.30	2.36
mES #33	0.76	1.96	10.95	17.50
hES_EWS	1.71	2.98	13.46	0.86
hES_KH	7.41	6.05	15.87	2.70
hCCS_KAS	2.16	3.16	16.58	28.85
hOS_U2OS	14.79	3.42	19.33	40.42

Probes), anti-mouse CD99 (a gift of Dietmar Vestweber, Max Planck Institute for Molecular Biomedicine, Muenster, Germany), anti-COL2A (Millipore), anti-S100 (Dako), anti-COL10 (SLS), anti-CD57 (Sigma-Aldrich), anti-NGFR (Millipore), anti-β-catenin (Becton Dickinson), anti-nestin (Chemicon), and anti-myosin (Nichirei). Immunofluorescent images were photographed with a Zeiss LSM 710 laser scanning microscope with a ×40 objective (Zeiss) and LSM Software ZEN 2009 (Zeiss).

Western blotting. Western blot analysis was performed using lysates of whole tumor tissues as described previously (54).

RT-PCR and real-time quantitative RT-PCR. Total RNA extraction, reverse transcription, and RNA quantification were performed according to methods described previously (54). Conventional RT-PCR and real-time quantitative RT-PCR were performed by using a Gene Amp 9700 thermal cycler (Applied Biosystems) and a 7500 Fast Real-Time PCR System (Applied Biosystems), respectively. The sequences of the oligonucleotide primers are shown in Supplemental Excel File 6.

Luciferase assay. A 1,340-bp genomic DNA fragment upstream from the murine *Gdf5* exon 1 was amplified by PCR using the following primers: forward (5′-TTCTATAATCCTACTCTGTAG-3′) and reverse (5′-CTGAAAATAACTCGTTCTTG-3′). The fragment was inserted into the pGL4.10 vector (Promega) and transfected into eSZ, eGP, eSyR, or trunk cells using Lipofectamine 2000 (Invitrogen). Luciferase assays were performed as described previously (54).

In vitro differentiation assay. Cells were plated at 2×10^5 cells per well in 6-well plates and cultured in growth medium. Adipogenic, chondrogenic, osteogenic, myogenic, and neurogenic differentiation assays were conducted according to the methods previously described (55–57).

Microarray analysis. GeneChip analysis was conducted to determine gene expression profiles. A per cell normalization method was applied to eSZ and eGP samples (58). Briefly, cellular lysates were prepared with RLT buffer (QIAGEN). After RNA cocktails were added to the cell lysates according to the amount of DNA, total RNA was extracted using the RNeasy Mini Kit (QIAGEN). The murine Genome 430 2.0 Array (Affymetrix) was hybridized with aRNA probes generated from eSZ and eGP cells and murine Ewing's sarcoma tissue. After staining with streptavidin-phycoerythrin conjugates, arrays were scanned using an Affymetrix GeneChip Scanner 3000 and analyzed using Affymetrix GeneChip Command Console Software (Affymetrix) and GeneSpring GX 11.0.2 (Agilent Technologies) as described previously (59). The expression data for eSZ and eGP cells were converted to mRNA copy numbers per cell by the Percellome method, quality controlled, and analyzed using Percellome software (58). GSEA was performed using GSEA-P 2.0 software (60).

Data comparisons and clustering between murine and human microarray data sets. The microarray data from 10 murine Ewing's sarcoma samples were compared with human microarray data sets. Data from the ONCOMINE database (https://www.oncomine.org/) were accessed in June 2011. Five microarray studies containing 117 tumor samples that were analyzed using Human Genome U133A Array (Affymetrix) were queried for gene expression. CEL files from E-MEXP-353 (61), E-MEXP-1142 (62), GSE6481 (63), GSE7529 (64), GSE21122 (65), GSE6461 (66), GSE42548 (67), GSE23972 (68), GSE20196 (69), and GSE10172 (70) were downloaded. The probe sets of the human U133A array were translated into 23,860 murine 430 2.0 arrays by the translation function of GeneSpring using Entrez Gene ID to make a novel common platform. Hierarchical clustering was achieved using log-transformed data and the following procedure. For the initial statistical analysis, 13,026 genes that showed a "present" or "marginal" call in at least 24 of a total of 32 human Ewing's sarcoma samples were selected. Then, 12,340 probes were selected by 1-way ANOVA ($P < 0.05$) analysis. Finally, 1,819 probes that showed >2-fold differences of expression in at least 3 tumor types were selected. With these 1,819 probes, hierarchical clustering was performed using the average linkage method and the Pearson's centered measurements. In addition, a probe set consisting of the 2,000 sequences that were the most altered in expression in human and mouse round cell tumors (Ewing's sarcoma, neuroblastoma, poorly differentiated synovial sarcoma, and malignant lymphoma) was used to distinguish each tumor from the other 3 using a fold-change analysis. Then, the frequencies of these 2,000 probes were compared between mouse Ewing's sarcoma and 4 human tumor types and between human Ewing's sarcoma and 4 mouse tumor types to find the closest tumor type using similar entities from GeneSpring.

ChIP. A total of 5×10^6 cells per immunoprecipitation were cross-linked with 10% formaldehyde for 10 minutes at room temperature. Histone immunoprecipitation was performed with anti-histone antibodies targeted against H3K9/K14Ac, H3K4/me3, H3K27/me3, total H3 (Cell Signaling Technologies), or H3K9/me3 (Millipore) preconjugated to protein G magnetic beads. Immunoprecipitated DNA was amplified with primers specific for each region. Sequences are shown in Supplemental Excel File 6.

Cre/loxP-mediated gene silencing. eSZ cells were transduced with a floxed *EWS-FLI1* retrovirus, and Ewing's sarcoma cells were obtained from a subcutaneous tumor developed in a nude mouse. Tumor cells were transduced with pMSCV-Cre-puro retrovirus in vitro. Senescence-associated β-galactosidase expression was detected using a Senescence Detection Kit (Biovision) 4 days after transduction of the retrovirus.

siRNA interference studies. For knockdown of *FLI1*, *Dkk2*, *Catnb*, *Prkcb1*, *Ezh2*, *Igf1*, *Dkk1*, and *Erg*, siRNAs were purchased from QIAGEN. The list of siRNAs is shown in Supplemental Excel File 7. siRNAs were introduced into mouse Ewing's sarcoma cells according to the manufacturer's protocol. Knockdown efficiencies were confirmed by Western blotting using anti-FLAG (Sigma-Aldrich), anti-ERG and anti-PKC β1 (Santa Cruz Biotechnology), anti-β-catenin (Becton Dickinson), and anti-EZH2 (Cell Signaling Technologies) or RT-PCR.

Pharmacological experiments with specific inhibitors. Mouse Ewing's sarcoma cells were treated with MEK1 inhibitor U0126 (Cell Signaling Technologies) in vitro. Both mouse and human Ewing's sarcoma cell lines were treated with WNT/β-catenin inhibitors, iCRT14 and PNU74654 (Tocris Bioscience); an EZH2 inhibitor, DZNeP (Cayman Chemical); or a PARP1 inhibitor, olaparib (Selleckchem), both in vitro and in vivo. Inhibition of ERG phosphorylation was examined by Western blotting using anti-P-ERK1/2 and anti-ERK1/2 (Cell Signaling

Technologies). For in vivo experiments, 1×10^6 tumor cells were transplanted subcutaneously into nude mice, and the mice were treated with specific inhibitors when the tumor diameter reached 5 mm. All the inhibitors were dissolved in 0.2% DMSO, and they were administered by intraperitoneal injection 3 times per week.

Cell cycle assay. Single-cell suspensions were permeabilized with 0.1% Triton X-100 in PBS, and 50 mg/ml propidium iodide and 1 mg/ml RNAse A were added. The cell suspensions were then analyzed by using a FACSCalibur flow cytometer and ModFit software (Becton Dickinson).

Cloning retroviral integration sites. Retroviral integration sites of individual mouse Ewing's sarcoma were isolated by inverse PCR, sequenced, and mapped as described previously (71).

Accession numbers. The microarray data sets are accessible through the NCBI Gene Expression Omnibus (GEO) database (http://www.ncbi.nlm.nih.gov/geo), with accession numbers GSE32615 and GSE32618.

Statistics. Continuous distributions were compared with 2-tailed Student's *t* test. Survival analysis was performed using the Kaplan-Meier life table method, and survival between groups was compared with the log-rank test. The 2-proportion *z* test was used to evaluate the significance of differences in the matched probe sets between 2 tumor types. All *P* values were 2 sided, and a *P* value of less than 0.05 was considered significant.

Study approval. Animals were handled in accordance with the guidelines of the animal care committee at the Japanese Foundation for Cancer Research, which gave ethical approval for these studies.

Acknowledgments

We thank W. Kurihara and T. Koui for helping with the microarray analyses; S.J. Baker (St Jude Children's Research Hospital, Memphis, Tennessee, USA) for EWS-FLI1 cDNA; and D. Vestweber (Max Planck Institute for Molecular Biomedicine, Muenster, Germany) for anti-mouse CD99. The research was funded by Grant-in-Aid for Scientific Research on Priority Areas Cancer 17013086 from Ministry of Education, Culture, Sports, Science and Technology and Grant-in-Aid for Young Scientists 23791672 from Japan Society for the Promotion of Science.

Received for publication July 29, 2013, and accepted in revised form April 10, 2014.

Address correspondence to: Takuro Nakamura, 3-8-31 Ariake, Koto-ku, Tokyo 135-8550, Japan. Phone: 81.3.3570.0462; Fax: 81.3.3570.0463; E-mail: takuro-ind@umin.net.

1. Bernstein M, et al. Ewing's sarcoma family of tumors: current management. *Oncologist.* 2006;11(5):503–519.
2. Ewing J. Diffuse endothelioma of bone. *Proc New York Pathol Soc.* 1921;21:17–24.
3. Hu-Lieskovan S, Zhang J, Wu L, Shimada H, Schofield DE, Triche TJ. EWS-FLI1 fusion protein up-regulates critical genes in neural crest development and is responsible for the observed phenotype of Ewing's family of tumors. *Cancer Res.* 2005;65(11):4633–4644.
4. Tirode F, Laud-Duval K, Prieur A, Delorme B, Cahrbord P, Delattre O. Mesenchymal stem cell features of Ewing tumors. *Cancer Cell.* 2007;11(5):421–429.
5. Delattre O, et al. Gene fusion with an ETS DNA-binding domain caused by chromosome translocation in human tumours. *Nature.* 1992;359(6391):162–165.
6. Zucman J, et al. Combinatorial generation of variable fusion proteins in the Ewing family of tumours. *EMBO J.* 1993;12(12):4481–4487.
7. Sorensen PH, Lessnick SL, Lopez-Terrada D, Liu XF, Triche TJ, Denny CT. A second Ewing's sarcoma translocation, t(21;22), fuses the EWS gene to another ETS-family transcription factor, ERG. *Nat Genet.* 1994;6(2):146–151.
8. Ordonez JL, Osuna D, Herrero D, de Alava E, Madoz-Gurpide J. Advances in Ewing's sarcoma research: where are we now and what lies ahead? *Cancer Res.* 2009;69(18):7140–7150.
9. Riggi N, et al. Development of Ewing's sarcoma from primary bone marrow-derived mesenchymal progenitor cells. *Cancer Res.* 2005;65(24):11459–11468.
10. Castillero-Trejo Y, Eliazer S, Xiang L, Richardson JA, Ilaria RL Jr. Expression of the EWS/FLI-1 oncogene in murine primary bone-derived cells results in EWS/FLI-1-dependent, Ewing sarcoma-like tumors. *Cancer Res.* 2005;65(19):8698–8705.
11. Arndt CAS, Crist WM. Common musculoskeletal tumors of childhood and adolescence. *N Engl J Med.* 1999;341(5):342–352.
12. Iwamoto M, et al. 2007. Transcription factor ERG and joint and articular cartilage formation during mouse limb and spine skeletogenesis. *Dev Biol.* 2007;305(1):40–51.
13. Koyama E, et al. A distinct cohort of progenitor cells participates in synovial joint and articular cartilage formation during mouse limb skeletogenesis. *Dev Biol.* 2008;316(1):62–73.
14. Mundy C, et al. Synovial joint formation requires local Ext1 expression and heparin sulfate production in developing mouse embryo limbs and spine. *Dev Biol.* 2011;351(1):70–81.
15. Ambros IM, Ambros PF, Strehl S, Kovar H, Gadner H, Salzer-Kuntschik M. MIC2 is a specific marker for Ewing's sarcoma and peripheral primitive neuroectodermal tumors. Evidence for a common histogenesis of Ewing's sarcoma and peripheral primitive neuroectodermal tumors from MIC2 expression and specific chromosome aberration. *Cancer.* 1991;67(7):1886–1893.
16. Bixel G, Kloep S, Butz S, Petri B, Engelhardt B, Vestweber D. Mouse CD99 participates in T-cell recruitment into inflamed skin. *Blood.* 2004;104(10):3205–3213.
17. Vortkamp A, Lee K, Lanske B, Segre GV, Kronenberg HM, Tabin CJ. Regulation of rate of cartilage differentiation by Indian Hedgehog and PTH-related protein. *Science.* 1996;273(5275):613–622.
18. Sohaskey ML, Yu J, Diaz MA, Plaas AH, Harland RM. JAWS coordinates chondrogenesis and synovial joint positioning. *Development.* 2008;135(13):2215–2220.
19. Vijayaraj P, et al. Erg is a crucial regulator of endocardial-mesenchymal transformation during cardiac valve morphogenesis. *Development.* 2012;139(21):3973–3985.
20. Storm EE, Kingsley DM. GDF5 coordinates bone and joint formation during digit development. *Dev Biol.* 1999;209(1):11–27.
21. St-Jacques B, Hammerschmidt M, McMahon AP. Indian hedgehog signaling regulates proliferation and differentiation of chondrocytes and is essential for bone formation. *Genes Dev.* 1999;13(16):2072–2086.
22. Mak KK, Kronenberg HM, Chuang PT, Mackem S, Yang Y. Indian hedgehog signals independently of PTHrP to promote chondrocyte hypertrophy. *Development.* 2008;135(11):1947–1956.
23. Toomey EC, Schiffman JD, Lessnick SL. Recent advances in the molecular pathogenesis of Ewing's sarcoma. *Oncogene.* 2010;29(32):4504–4516.
24. James CG, Stanton LA, Agoston H, Ulici V, Underhill TM, Beier F. Genome-wide analyses of gene expression during mouse endochondral ossification. *PLoS One.* 2010;5(1):e8693.
25. Honsei N, Ikuta T, Kawana K, Kaneko Y, Kawajiri K. Participation of nuclear localization signal 2 in the 3′-ETS domain of FLI1 in nuclear translocation of various chimeric EWS-FLI1 oncoproteins in Ewing tumor. *Int J Oncol.* 2006;29(3):689–693.
26. Miyagawa Y, et al. EWS/ETS regulates the expression of the Dickkopf family in Ewing family tumor cells. *PLoS One.* 2009;4(2):e4634.
27. Surdez D, et al. Targeting the EWSR1-FLI1 oncogene-induced protein kinase PKC-β abolishes Ewing sarcoma growth. *Cancer Res.* 2012;72(17):4494–4503.
28. Richter GH, et al. EZH2 is a mediator of EWS/FLI1 driven tumor growth and metastasis blocking endothelial and neuro-ectodermal differentiation. *Proc Natl Acad Sci U S A.* 2009;106(13):5324–5329.
29. Nishimori H, et al. The Id2 gene is a novel target of transcriptional activation by EWS-ETS fusion proteins in Ewing family tumors. *Oncogene.* 2002;21(54):8302–8309.
30. Smith R, et al. Expression profiling of EWS/FLI1 identifies NKX2.2 as a critical target gene in Ewing's sarcoma. *Cancer Cell.* 2006;9(5):405–416.
31. Kinsey M, Smith R, Lessnick SL. NR0B1 is required for the oncogenic phenotype mediated by EWS/FLI in Ewing's sarcoma. *Mol Cancer Res.* 2006;4(11):851–859.
32. Abaan OD, Levenson A, Khan O, Furth PA, Uren A, Toretsky JA. PTPL1 is a direct transcriptional target of EWS-FLI1 and modulates Ewing's sarcoma tumorigenesis. *Oncogene.* 2005;24(16):2715–2722.
33. Wakahara K, et al. EWS-Fli1 up-regulates expression of the Aurora A and Aurora B kinases. *Mol Cancer Res.* 2008;6(12):1937–1945.
34. Luo W, Gangwal K, Sankar S, Boucher KM, Thomas D, Lessnick SL. GSTM4 is a microsatellite-containing EWS/FLI target involved in Ewing's sarcoma oncogenesis and therapeutic resistance. *Oncogene.* 2009;28(46):4126–4132.
35. Fuchs B, Inwards C, Scully SP, Janknecht R. hTERT is highly expressed in Ewing's sarcoma and activated by EWS-ETS oncoproteins. *Clin Orthop Relat Res.* 2004;426(426):64–68.
36. Watanabe G, et al. Induction of tenascin-C by tumor-specific EWS-ETS fusion genes. *Genes Chromosomes Cancer.* 2003;36(3):224–232.
37. Deneen B, Hamidi H, Denny CT. Functional analysis of the EWS/ETS target gene uridine phosphorylase. *Cancer Res.* 2003;63(14):4268–4274.
38. Hahm KB, et al. Repression of the gene encoding the TGF-beta type II receptor is a major target of the EWS-FLI1 oncoprotein. *Nat Genet.* 1999;23(2):222–227.
39. Dohjima T, Ohno T, Banno Y, Nozawa Y, Wen-yi Y, Shimizu K. Preferential down-regulation of phospholipase C-beta in Ewing's sarcoma cells transfected with antisense EWS-Fli-1. *Br J Cancer.* 2000;82(1):16–19.
40. Scotlandi K, et al. Insulin-like growth factor I receptor-mediated circuit in Ewing's sarcoma/peripheral

neuroectodermal tumor: a possible therapeutic target. *Cancer Res.* 1998;56(20):4570–4574.
41. Balamuth NJ, Womer RB. Ewing's sarcoma. *Lancet Oncol.* 2010;11(2):184–192.
42. Niehrs C. Function and biological roles of the Dickkopf family of Wnt modulators. *Oncogene.* 2006;25(57):7469–7481.
43. Mikheev AM, Mikheeva SA, Liu B, Cohen P, Zarbl H. A functional genomics approach for the identification of putative tumor suppressor genes: Dickkopf-1 as suppressor of HeLa cell transformation. *Carcinogenesis.* 2004;25(1):47–59.
44. Uren A, Wolf V, Sun YF, Azari A, Rubin JS, Toretsky JA. Wnt/Frizzled signaling in Ewing sarcoma. *Pediatr Blood Cancer.* 2004;43(3):243–249.
45. Garnett MJ, et al. Systematic identification of genomic markers of drug sensitivity in cancer cells. *Nature.* 2012;483(7391):570–575.
46. Deneen B, Denny CT. Loss of p16 pathways stabilizes EWS/FLI1 expression and complements EWS/FLI1 mediated transformation. *Oncogene.* 2001;20(46):6731–6741.
47. Sohn EJ, Li H, Reldy K, Beers LF, Christensen BL, Lee SB. EWS/FLI1 oncogene activates caspase 3 transcription and triggers apoptosis in vivo. *Cancer Res.* 2010;70(3):1154–1163.
48. Riggi N, et al. EWS-FLI-1 modulates miRNA145 and SOX2 expression to initiate mesenchymal stem cell reprogramming toward Ewing sarcoma cancer stem cells. *Genes Dev.* 2010;24(9):916–932.
49. Grier HE. The Ewing family of tumors: Ewing's sarcoma and primitive neuroectodermal tumors. *Pediatr Clin North Am.* 1997;44(4):991–1004.
50. Soliman H, Ferrari A, Thomas D. Sarcoma in the young adult population: An international view. *Sem Oncol.* 2009;36(3):227–236.
51. Martins AS, et al. A pivotal role for heat shock protein 90 in Ewing sarcoma resistance to anti-insulin-like growth factor 1 receptor treatment: in vitro and in vivo study. *Cancer Res.* 2008;68(15):6260–6270.
52. Glade Bender JL, et al. Phase I pharmacokinetic and pharmacodynamics study of pazopanib in children with soft tissue sarcoma and other refractory solid tumors: a children's oncology group phase I consortium report. *J Clin Oncol.* 2013;31(24):3034–3043.
53. Jin G, et al. Trib1 and Evi1 cooperate with Hoxa and Meis1 in myeloid leukemogenesis. *Blood.* 2007;109(9):3998–4005.
54. Kawamura-Saito M, et al. Fusion between CIC and DUX4 up-regulates PEA3 family genes in Ewing-like sarcomas with t(4;19)(q35;q13) translocation. *Hum Mol Genet.* 2006;15(13):2125–2137.
55. Pittenger MF, et al. Multilineage potential of adult human mesenchymal stem cells. *Science.* 1999;284(5411):143–147.
56. Sakaguchi Y, Sekiya I, Yagishita K, Muneta T. Comparison of human stem cells derived from various mesenchymal tissues: superiority of synovium as a cell source. *Arthritis Rheum.* 2005;52(8):2521–2529.
57. Shiota M, et al. Isolation and characterization of bone marrow-derived mesenchymal progenitor cells with myogenic and neuronal properties. *Exp Cell Res.* 2007;313(5):1008–1023.
58. Kanno J, et al. "Per cell" normalization method for mRNA measurement by quantitative PCR and microarrays. *BMC Genomics.* 2006;7:64.
59. Fujino T, et al. Function of EWS-POU5F1 in sarcomagenesis and tumor cell maintenance. *Am J Pathol.* 2010;176(4):1973–1982.
60. Subramanian A, Kuehn H, Gould J, Tamayo P, Mesirov JP. GSEA-P: a desktop application for gene set enrichment analysis. *Bioinformatics.* 2007; 23(23):3251–3253.
61. Henderson SR, et al. A molecular map of mesenchymal tumors. *Genome Biol.* 2005;6(9):R76.
62. Schaefer KL, et al. Microarray analysis of Ewing's sarcoma family of tumours reveals characteristic gene expression signatures associated with metastasis and resistance to chemotherapy. *Eur J Cancer.* 2008;44(5):699–709.
63. Nakayama R, et al. Gene expression analysis of soft tissue sarcomas: characterization and reclassification of malignant fibrous histiocytoma. *Mod Pathol.* 2007;20(7):749–759.
64. Albino D, et al. Identification of low intratumoral gene expression heterogeneity in neuroblastic tumors by genome-wide expression analysis and game theory. *Cancer.* 2008;113(6):1412–1422.
65. Barretina J, et al. Subtype-specific genomic alterations define new targets for soft-tissue sarcoma therapy. *Nat Genet.* 2010;42(8):715–721.
66. Haldar M, et al. A conditional mouse model of synovial sarcoma: insights into a myogenic origin. *Cancer Cell.* 2007;11(4):375–388.
67. Teitz T, et al. Th-MYCN mice with caspase-8 deficiency develop advanced neuroblastoma with bone marrow metastasis. *Cancer Res.* 2013;73(13):4086–4097.
68. Jeannet R, et al. Oncogenic activation of the Notch1 gene by deletion of its promoter in Ikaros-deficient T-ALL. *Blood.* 2010;115(25):5443–5454.
69. Nakayama R, et al. Gene expression profiling of synovial sarcoma: distinct signature of poorly differentiated type. *Am J Surg Pathol.* 2010;34(11):1599–1607.
70. Masque-Soler N, Szczepanowski M, Kohler CW, Spang R, Klapper W. Molecular classification of mature aggressive B-cell lymphoma using digital multiplexed gene expression on formalin-fixed paraffin-embedded biopsy specimens. *Blood.* 2013; 122(11):1985–1986.
71. Tanaka M, Jin G, Yamazaki Y, Takahara T, Takuwa M, Nakamura T. Identification of candidate cooperative genes of the Apc mutation in transformation of the colon epithelial cell by retroviral insertional mutagenesis. *Cancer Sci.* 2008;99(5):979–985.

© 2014. Published by The Company of Biologists Ltd | Development (2014) 141, 2260-2270 doi:10.1242/dev.103705

RESEARCH ARTICLE

Active repression by RARγ signaling is required for vertebrate axial elongation

Amanda Janesick[1], Tuyen T. L. Nguyen[1], Ken-ichi Aisaki[2], Katsuhide Igarashi[2], Satoshi Kitajima[2], Roshantha A. S. Chandraratna[3], Jun Kanno[2] and Bruce Blumberg[1,4,*]

ABSTRACT

Retinoic acid receptor gamma 2 (RARγ2) is the major RAR isoform expressed throughout the caudal axial progenitor domain in vertebrates. During a microarray screen to identify RAR targets, we identified a subset of genes that pattern caudal structures or promote axial elongation and are upregulated by increased RAR-mediated repression. Previous studies have suggested that RAR is present in the caudal domain, but is quiescent until its activation in late stage embryos terminates axial elongation. By contrast, we show here that RARγ2 is engaged in all stages of axial elongation, not solely as a terminator of axial growth. In the absence of RA, RARγ2 represses transcriptional activity *in vivo* and maintains the pool of caudal progenitor cells and presomitic mesoderm. In the presence of RA, RARγ2 serves as an activator, facilitating somite differentiation. Treatment with an RARγ-selective inverse agonist (NRX205099) or overexpression of dominant-negative RARγ increases the expression of posterior Hox genes and that of marker genes for presomitic mesoderm and the chordoneural hinge. Conversely, when RAR-mediated repression is reduced by overexpressing a dominant-negative co-repressor (c-SMRT), a constitutively active RAR (VP16-RARγ2), or by treatment with an RARγ-selective agonist (NRX204647), expression of caudal genes is diminished and extension of the body axis is prematurely terminated. Hence, gene repression mediated by the unliganded RARγ2–co-repressor complex constitutes a novel mechanism to regulate and facilitate the correct expression levels and spatial restriction of key genes that maintain the caudal progenitor pool during axial elongation in *Xenopus* embryos.

KEY WORDS: Active repression, Axial elongation, Chordoneural hinge, Posterior Hox, Presomitic mesoderm, Retinoic acid receptor

INTRODUCTION

Repression mediated through unliganded retinoic acid receptors (RARs) is an important yet understudied function exhibited by nuclear receptors (reviewed by Weston et al., 2003). Although RA plays a major role in patterning the hindbrain, retina, placodes and somites, its absence is crucial for the development of structures found at the head and tail of the embryo. RARs exhibit basal repression in the absence of ligand, binding constitutively to their targets, recruiting co-repressors, and actively repressing the basal transcriptional machinery (Chen and Evans, 1995). When ligand is present, co-repressors are replaced by co-activators and target genes are transcribed (Chakravarti et al., 1996).

We previously demonstrated that repression mediated through unliganded RARs was important for anterior neural patterning, establishing a novel role for RAR as a repressor *in vivo* (Koide et al., 2001). Overexpression of a dominant-negative RARα expanded anterior and midbrain markers caudally and shifted somitomeres rostrally (Blumberg et al., 1997; Moreno and Kintner, 2004). Exogenous RA, constitutively active RARα or derepression of RARα produced the opposite effect: severe anterior truncations, diminished anterior markers, and anteriorly shifted midbrain and hindbrain markers. Stabilization of co-repressors resulted in enhanced anterior neural structures and posteriorly shifted mid/hindbrain markers (Koide et al., 2001).

Axial elongation requires continual replenishing of bipotential caudal progenitor cells (maintained by Wnt and FGF signaling, but inhibited by RA) that give rise to notochord, neural tube and somites (Cambray and Wilson, 2002; Davis and Kirschner, 2000). The most stem-like cells are located in the chordoneural hinge (CNH), where the posterior neural plate overlies the caudal notochord (Beck and Slack, 1998). Cells from the CNH contribute to presomitic mesoderm (PSM), which supplies committed somitic precursor cells to the rostral determination wavefront (reviewed by Dequeant and Pourquie, 2008). PSM is initially homogenous and unorganized [expressing *Mesogenin1* (*Msgn1*) and *Tbx6*], then becomes patterned into somitomeres marked by *Thylacine2* (*Thyl2*) and *Ripply2* (reviewed by Dahmann et al., 2011). Epithelialization of presomitic domains results in mature somites (Nakaya et al., 2004).

RA is well known to function in the trunk, where it promotes differentiation of PSM into somitomeres (Moreno and Kintner, 2004). By contrast, RA is actively metabolized and cleared by CYP26A1 in the caudal region (Fujii et al., 1997). Treatment with RA leads to loss of posterior structures (Sive et al., 1990); *Cyp26a1*$^{-/-}$ mice exhibit posterior truncations and homeotic vertebral transformations (Abu-Abed et al., 2001; Sakai et al., 2001). Exposing embryos to RA inhibits proliferation of axial progenitor cells in CNH and PSM, leading to axial truncation from premature exhaustion of the progenitor pool (Gomez and Pourquie, 2009). Therefore, RA is normally excluded from unsegmented mesenchyme in PSM and the CNH. RARγ is expressed at high levels throughout the entire caudal region, including CNH and PSM (Mollard et al., 2000; Pfeffer and De Robertis, 1994), yet, based on *Cyp26a1* expression, RA is absent (de Roos et al., 1999). The physiological significance of RARγ expression in the embryonic posterior is uncertain. RARγ might function to terminate the body axis at late stages by inducing apoptosis (Olivera-Martinez et al., 2012), but that model would not explain the strong expression of RARγ observed at neurula, continuing through tailbud stages, despite the apparent absence of RA.

[1]Department of Developmental and Cell Biology, 2011 Biological Sciences 3, University of California, Irvine, CA 92697-2300, USA. [2]Division of Cellular and Molecular Toxicology, Biological Safety Research Center, National Institute of Health Sciences, 1-18-1 Kamiyoga, Setagaya-ku, Tokyo 158-8501, Japan. [3]IO Therapeutics, Santa Ana, CA 92705-5851, USA. [4]Department of Pharmaceutical Sciences, University of California, Irvine, CA 92697-2300, USA.

*Author for correspondence (blumberg@uci.edu)

Received 29 September 2013; Accepted 27 March 2014

Development (2014) 141, 2260-2270 doi:10.1242/dev.103705

Rarγ2 skirts the posterior edge of the determination wavefront and is co-expressed with PSM, CNH and posterior Hox markers. We hypothesized that *Rarγ2* serves a dual function: as an activator in somite differentiation but a repressor in the maintenance of PSM and the caudal progenitor pool. Loss of RARγ2 severely shortens the embryo body axis and inhibits somitogenesis. Loss of RARγ2 expands the anterior border of PSM expression near the wavefront (where activation is lost), but diminishes the expression domain of caudal PSM and posterior Hox genes (where repression is lost). Increasing RAR-mediated repression expands the expression of posterior Hox, PSM and CNH markers, creating smaller somitomere domains via an indirect, 'repressing a repressor' mechanism. Relief of repression results in a truncated body axis with decreased PSM and CNH markers. Axial extension and segmentation in vertebrates relies on the maintenance of unsegmented PSM mesenchyme and replenishing of caudal progenitor cells. Our data show that RARγ2 plays a crucial role in this process, repressing target genes to maintain PSM and caudal progenitors in the absence of RA, while activating others to promote somitogenesis in the presence of RA.

RESULTS

Posterior Hox, PSM and CNH genes are upregulated by RAR inverse agonist

We showed previously that active repression of RAR target genes by unliganded RAR is required for head formation (Koide et al., 2001). Treatment with the pan-RAR inverse agonist AGN193109 increased the expression of genes involved in patterning anterior neural structures, whereas treatment with pan-RAR agonist TTNPB decreased the expression of anterior marker and cement gland-specific genes (Koide et al., 2001), revealing a set of genes specifically upregulated/downregulated by TTNPB (Arima et al., 2005). Validation studies identified a subset upregulated by AGN193109. We hypothesized that active repression by unliganded RARs is biologically important and designed an experiment to identify genes upregulated or downregulated by modulating repression. Percellome analysis (Kanno et al., 2006) quantified the copy number per embryo of all genes represented on Affymetrix *Xenopus* microarray v1.0. Among these we identified a collection of genes linked to the maintenance of caudal axial progenitors that were downregulated by TTNPB and upregulated by AGN193109 (Table 1). RAR-mediated repression upregulates the steady-state expression of posterior Hox paralogs 9-13 and genes found in both unsegmented PSM and CNH. Thus, we hypothesized that RAR is a repressor required for axial elongation.

Xenopus RARs repress basal transcription in the absence of ligand

The ability of unliganded RARs to behave as repressors is well documented, although not all human receptor subtypes can recruit co-repressors (e.g. SMRT) in the absence of ligand (Wong and Privalsky, 1998). We tested the ability of *Xenopus* RAR (xRAR) subtypes to repress basal activity of a luciferase-dependent reporter using the GAL4-RAR system (supplementary material Fig. S1D-F) (Blumberg et al., 1996). *Xenopus* RARα, RARβ and RARγ suppressed basal activity *in vitro* and *in vivo* (supplementary material Fig. S1A,C), whereas human RARβ and RARγ did not (supplementary material Fig. S1B). Thus, xRARs can function as repressors in the absence of ligand.

Rarγ2 is expressed in the PSM and CNH but is mostly absent from the trunk

Whole-mount *in situ* hybridization (WISH) revealed that *Rarγ2* is the predominant isoform expressed in the *Xenopus* embryonic posterior (supplementary material Fig. S2A). In late neurula and early tailbud stage embryos, *Rarγ2* is strongly expressed in the anterior and posterior, but almost undetectable in the trunk. *Rarγ2* expression later becomes pronounced in the tail and head, particularly in hyoid, branchial and mandibular neural crest. *Rarγ1* is expressed similarly. QPCR analysis revealed that *Rarγ2* is 1000- to 4000-fold more abundant than *Rarγ1* at stages 10-22, and 100- to 400-fold more abundant at all other stages analyzed (supplementary material Fig. S2B). Subsequent experiments utilized *Rarγ2*-selective reagents. We conclude that *Rarγ2* is the predominant isoform expressed in the posterior region of embryos.

Rarγ2 is expressed where RA is probably absent (owing to CYP26A1 expression). Key posterior genes were upregulated by AGN193109. We hypothesized that RARγ2 posterior to the wavefront is a repressor, maintaining unsegmented PSM and the progenitor cell pool required for axial elongation. We used double WISH to compare the expression of *Rarγ2* with that of *Hoxc10*, an important member of the Abd-B Hox gene family promoting caudal development over thorax (Lamka et al., 1992). *Rarγ2* expression completely overlaps caudal *Hoxc10* expression (Fig. 1E,H) but not the anteriormost neural or lateral plate expression of *Hoxc10* (Fig. 1E,H). These data position

Table 1. Percellome analysis reveals that posterior Hox, PSM and CNH markers are upregulated by RAR inverse agonist

Unigene	109 (fold)	*P*	TTN (fold)	*P*	Symbol	Gene name	Cat
Xl.72193	3.57	2.11×10^{-3}	0.19	5.77×10^{-4}	*Hoxc13*	Homeobox C13	PP
Xl.266	3.47	4.26×10^{-3}	0.12	2.26×10^{-4}	*Hoxa11*	Homeobox A11	PP
Xl.21864	3.15	2.03×10^{-3}	0.22	2.68×10^{-4}	*Hoxc10*	Homeobox C10	PP
Xl.72292	3.02	7.32×10^{-3}	0.16	1.62×10^{-4}	*Hoxd9*	Homeobox D9	PP
Xl.9560	2.73	9.74×10^{-4}	0.40	5.98×10^{-3}	*Hoxa9*	Homeobox A9	PP
Xl.12067	2.80	8.05×10^{-3}	0.18	2.51×10^{-5}	*Esr2*	Enhancer of Split related 2	PSM
Xl.29033	2.79	9.31×10^{-4}	0.26	1.62×10^{-5}	*Esr9*	Enhancer of Split related 9	PSM
Xl.78953	2.90	4.29×10^{-4}	0.37	2.68×10^{-3}	*Tbx6*	T-box gene Tbx6	PSM
Xl.483	2.53	4.18×10^{-3}	0.17	3.36×10^{-8}	*Msgn1*	Mesogenin 1	PSM
Xl.14524	2.32	2.76×10^{-2}	0.42	1.46×10^{-2}	*Esr5*	Enhancer of Split related 5	PSM
Xl.933	2.49	4.46×10^{-2}	0.40	2.73×10^{-2}	*xBra3*	T2, Brachyury homolog	CNH
Xl.1066	2.44	4.31×10^{-2}	0.34	2.09×10^{-3}	*xNot*	Notochord homeobox	CNH
Xl.457	3.10	1.37×10^{-3}	0.02	2.81×10^{-7}	*Derriere*	Growth differentiation factor 3	NC
Xl.16206	2.43	7.64×10^{-3}	0.27	2.35×10^{-6}	*Pnp*	Purine nucleoside phosphorylase	NC

Blastula stage embryos were soaked in 1 μM RAR agonist TTNPB (TTN), 1 μM RAR inverse agonist AGN193109 (109) or vehicle control (0.1% ethanol) until harvesting at stage 18. Cat, expression category: PP, posterior patterning; PSM, presomitic mesoderm; CNH, chordoneural hinge; NC, expression not characterized. Fold induction or reduction is relative to control vehicle. *P*-values were generated using CyberT.

Development (2014) 141, 2260-2270 doi:10.1242/dev.103705

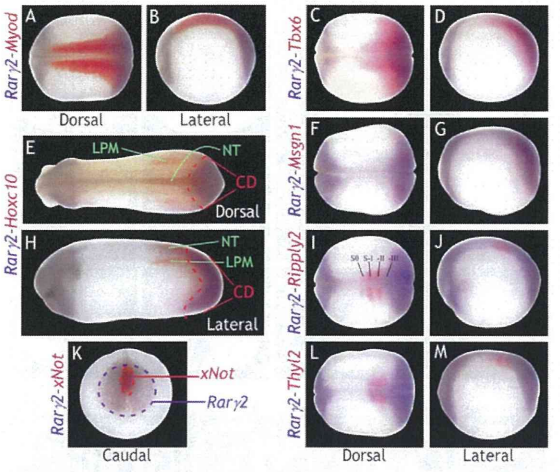

Fig. 1. Double WISH reveals the spatial relationship between *Rarγ2* and posterior Hox, PSM and CNH genes. (A-M) *Rarγ2* is stained with BM Purple and the other genes are stained with Fast Red. *Rarγ2* is caudal to *Myod* and *Tbx6* (A-D), but synexpressed with *Msgn1* (F,G) in neurula stage *Xenopus* embryos. (E,H) *Rarγ2* is synexpressed with the caudal domain (CD) of *Hoxc10* but not with neural tube (NT) or lateral plate mesoderm (LPM) of *Hoxc10* in tailbud stage embryos. *Rarγ2* overlaps with S–III domains of *Ripply2* (I,J) and *Thyl2* (L,M) expression, but not with more anterior somitomeres (S–II, S–I, S0). (K) *Rarγ2* overlaps with *xNot* expression in neurula stage embryos. Dorsal and lateral views shown with anterior to the left, except in K (caudal view with dorsal at top).

Rarγ2 as a potential regulator of posterior Hox genes and the caudal body plan.

We next defined the anterior limit of *Rarγ2* expression relative to the determination wavefront. *Myod* is a general muscle marker abutting and partially overlapping *Rarγ2* expression (Fig. 1A,B). *Thyl2* and *Ripply2* mark somitomeres, which are prepatterned PSM domains containing non-epithelialized, immature somites (Tam et al., 2000). *Thyl2* and *Ripply2* are only expressed in newly forming somitomeres and are assigned negative Roman numerals (S–I, S–II, etc.) versus mature somites (SI, SII, etc.) (Pourquie and Tam, 2001). *Msgn1* (Buchberger et al., 2000) is expressed caudal to *Thyl2* and *Ripply2*, marking non-patterned PSM-containing cells committed to the somitic fate (Nowotschin et al., 2012). *Tbx6* is also expressed in PSM, but unlike *Msgn1* its expression domain overlaps with somitomeres (Hitachi et al., 2008). *Rarγ2* and *Msgn1* are synexpressed at neurula (Fig. 1F,G) and tailbud (supplementary material Fig. S3) stages; *Tbx6* expression overlaps *Rarγ2* but extends rostrally beyond the *Rarγ2* domain (Fig. 1C,D; supplementary material Fig. S3). Anterior expression of *Rarγ2* mRNA ends at an RA-responsive region (supplementary material Fig. S4), coinciding with the most posterior somitomere domain (S–III) of *Thyl2* or *Ripply2* (Fig. 1I-M), thus skirting the posterior edge of the wavefront.

xNot, a notochord marker that regulates trunk and tail development, is concentrated in the extreme posterior notochord and floor plate by late neurula (von Dassow et al., 1993) and is often employed as a CNH marker in *Xenopus* (Beck and Slack, 1998) to reveal the location of bipotential stem cells (Cambray and Wilson, 2007; Takemoto et al., 2011). *xNot* is co-expressed with *Rarγ2* (Fig. 1K), agreeing with data suggesting that *Rarγ2* is present in CNH (Pfeffer and De Robertis, 1994). The double WISH data are consistent with *Rarγ2* functioning as an activator near where RA is present at the wavefront, yet as a repressor where it coincides with *Msgn1*, *xNot* and *Cyp26a1*.

RARγ-selective chemicals modulate activation or repression by RARγ

To separate the effects of RARγ in the posterior from RARα in the trunk, we characterized RARγ-selective agonist NRX204647 (4647) (Shimono et al., 2011; Thacher et al., 2000) and RARγ-selective inverse agonist NRX205099 (5099) (Tsang et al., 2003) in *Xenopus* embryos. Like AGN193109, 5099 is an inverse agonist, reducing RARγ signaling activity below basal levels by stabilizing the co-repressor complex bound to RARγ. Embryos treated with 1 μM agonist 4647 become primarily trunk (no head or tail structure), while 0.1 μM perturbs axial elongation (supplementary material Fig. S5), producing anterior truncations characteristic of RAR activators (Sive et al., 1990). Inverse agonist 5099 at 1 μM delayed development, producing enlarged heads and shortened trunks; half the dose elicited similar but weaker phenotypes, with effects absent at 0.1 μM (supplementary material Fig. S5). Treating neurula embryos significantly reduced severity but did not eliminate the phenotype (supplementary material Fig. S5).

To test the effects of these chemicals *in vivo* without interference from endogenous RARs, we mutated the DNA-binding specificity of a full-length RAR, $RAR^{EGCKG\rightarrow GSCKV}$. The mutant receptor recognizes a mutant TK-luc reporter, $(RXRE^{1/2}\text{-}GRE^{1/2})\times4$ TK-luc, to which endogenous RARs do not bind (Klein et al., 1996). In transient transfection assays, 4647 selectively activated RARγ at doses below 0.1 μM (supplementary material Fig. S6A). Similarly, 5099 selectively antagonized 10 nM 9-cis RA activation of RARγ below 0.1 μM (supplementary material Fig. S6B). We conclude that 4647 and 5099 behave as subtype-selective ligands to activate or repress RARγ.

RARγ-selective chemicals affect posterior Hox genes, PSM and somitomeres

We hypothesized that 4647 treatment of embryos would decrease posterior Hox gene expression and markers of PSM, whereas 5099 would produce the opposite effect. Microarray analysis (Table 1) revealed that *Hoxc13* and *Hoxc10* expression was upregulated by inverse agonist AGN193109 and downregulated by agonist TTNPB. We infer that increased expression of *Hoxc13* and *Hoxc10* results from RAR repressing the expression of a repressor of their expression. The expression pattern of *Hoxc13* (supplementary material Fig. S7) was not previously characterized.

We began soaking embryos in RARγ-selective doses of 4647, 5099 or vehicle control after gastrulation (stage 12.5) to focus on axial elongation. Treatment with 10 nM 4647 resulted in diminished caudal structures at stage 40 (supplementary material Fig. S5), reducing expression domains of *Hoxc10*, *Hoxd10* and *Hoxc13* (Fig. 2A-C). Conversely, treatment with 0.5 μM 5099 expanded their neural and lateral domains (Fig. 2A-C). To determine short-term effects of chemical treatments, we soaked embryos for 1 h at various stages and evaluated *Hoxc10* expression (supplementary material Fig. S8) and that of *Tbx6* (not shown) at stage 22. Repression by 5099 is required at early neurula, whereas activation by 4647 is required at mid- and late neurula stages for expected expansion and reduction, respectively, of *Hoxc10* expression (supplementary material Fig. S8). Higher, non-receptor-selective doses exacerbated effects on posterior Hox genes (supplementary material Fig. S9), suggesting that RARγ2 is the primary mediator. *Hoxc10* nearly abuts *Krox20*, demonstrating trunk shortening in 5099-treated embryos (supplementary material Fig. S9G,H). High